JOURNAL OF MATERIALS SCIENCE 23 (1988) 3578–3587

Instability during high strain rate compression of 2024 T351 aluminium

ROBERT G. O'DONNELL, RAYMOND L. WOODWARD
Australian Department of Defence, Materials Research Laboratories, PO Box 50, Ascot Vale, Victoria 3032, Australia

The flow behaviour of 2024 aluminium during drop weight compression tests was investigated. Use of cylindrical specimens of different height to diameter ratios, of different orientations and having undergone varying levels of prestrain, enabled the development of shear bands occuring within these specimens to be studied. The shear surfaces display a conical geometry and appear to develop in the presence of thermal softening after a flow stress maximum has been reached. Fracture along these surfaces appears to be associated with the rotation of strings of inclusions into the plane of the surface as well as severe deformation along the bands which leads to both thermal softening and exhaustion of matrix material ductility.

1. Introduction

Instabilities and flow localizations are features of metalworking and high-speed metal deformation processes which lead to both limitations in ductility and local non-uniformity of properties and structure. The occurrence of shear banding and its influence on isothermal bulk and sheet forming processes have been reviewed by Semiatin and co-workers [1, 2]. In both these studies and several other publications [3–7] the phenomenon of adiabatic shear has been reviewed. The present work focuses on the occurrence of an instability observed in drop weight compression testing of cylinders of the aluminium alloy 2024 T351. The phenomenon manifests itself as a drop in the load–displacement curve and is associated with metallographic evidence of shear banding in the samples.

Semiatin *et al.* [2] show that the condition for flow localization under isothermal conditions can be written as

$$\alpha = -\frac{1}{\dot{\varepsilon}}\frac{\mathrm{d}\dot{\varepsilon}}{\mathrm{d}\varepsilon} = \frac{\gamma' - 1}{m} \tag{1}$$

where

$$\gamma' = \left(\frac{1}{\sigma}\frac{\mathrm{d}\sigma}{\mathrm{d}\varepsilon}\right)_{\dot{\varepsilon}} = \left[\left(\frac{\partial\sigma}{\partial\varepsilon}\right)_{\dot{\varepsilon},T}\mathrm{d}\varepsilon + \left(\frac{\partial\sigma}{\partial T}\right)_{\varepsilon,\dot{\varepsilon}}\mathrm{d}T\right]\Big/\sigma\mathrm{d}\varepsilon \tag{2}$$

α is the flow localization parameter, m is the strain-rate hardening index $= (\partial \ln \sigma/\partial \ln \dot{\varepsilon})$, ε and $\dot{\varepsilon}$ are strain and strain rate, T is temperature, and σ is flow stress.

Flow localization should be observed when $\alpha = 0$; however, in practice it becomes noticeable with some significant positive value of α. The condition can be simplified for specific cases and, in particular, for the case of negligible strain-rate sensitivity and planar flow conditions, where slip lines are observed, it is equivalent to the condition for adiabatic shear failure proposed for Zener and Holloman [8], and Recht [9], and simplified by Staker [10] for the case where thermal conduction was negligible. Semiatin and co-workers [2, 11, 12] have shown that a flow stress maximum is a necessary condition for shear band occurrence and flow localization; however, this alone was not sufficient and a substantial degree of flow softening (negative strain hardening) must occur before noticeable flow localization occurs. Load/stroke curves can have a positive slope whilst shear banding develops [13].

Under conditions of uniaxial compression there have been many studies of the development of flow geometry [1, 14] and limitations due to fracture [15, 16]. In particular Mescall *et al.* [14] have shown how strain concentrations can develop by rotation of the sides of the sample to meet the die under conditions of limiting friction. The occurrence of shear banding in the form of a cross and the rotation of the bands as a function of strain has been outlined by Semiatin and Jonas [1]. Under rapid uniaxial compression, failure of samples has been attributed to the development of adiabatic shear bands in a characteristic geometric pattern [17, 18]. Adiabatic heating can also lead to a general softening without localization in such testing [19].

Fractures have been observed in planar, as well as axisymmetric, compression processes and can be associated with velocity discontinuities and sliplines [20, 21]. Watts and Ford [22] demonstrated the occurrence of maxima and minima in the flow stress in plane strain compression tests, associated with the variation of the slipline field with height/width ratio.

The shear banding observed in the present axisymmetric compression test was essentially in the form of a conical surface and initiated when the height to

0022–2461/88 $03.00 + .12

TABLE I Influence of temperature and specimen orientation

Test temperature (°C)	Orientation*, behaviour† and (strain at instability)‡					
	O	A	B	C	D	E
0	R S (0.83) R					
20	T (0.76) T (0.70) T (0.70) T (0.85)	R T (0.87)	T (0.79) R T (0.74)	T (0.74) T (0.74) T (0.94)	T (0.72) T (0.86) R	T (0.78) T (0.80) T (0.64)
50	S (0.75) T (0.71) T (0.78) T (0.86)	R T (0.91)	S (0.75) R	R T (0.82)	R T (0.89)	R T (0.87)
90	R T (0.79)					

*Orientation definitions: Plate O, through thickness (Short Transverse)
A, rolling direction
B, long transverse

Bar C, axial
D, circumferential
E, radial

†Behaviour definitions – see Fig. 1: R, continuous increase in load
S, levelling of load/displacement curve
T, dip in load/displacement curve

‡Figures in parentheses represent the observed strain at instability in the load/displacement curve.

diameter ratio was 0.5. By examining the influence of temperature, prestrain, sample orientation and geometry on its occurrence, and the appearance of the load/displacement and derived stress/strain curves, the sequence of events leading to the instability is elucidated.

2. Experimental procedure

Cylindrical compression specimens, 4.76 mm diameter and of varying heights, were machined from 2024 aluminium in the T351 condition. Specimens were removed from both plate and bar stock at different orientations (see Table I), to observe the effects which may be attributed to texture, chemical segregation or the orientation of undissolved intermetallic particles. However, for most tests the samples were taken with their axis in the through thickness (short transverse) direction of the plate material, and this applies unless specifically stated otherwise below.

Initial strain rates of 600 sec^{-1} were obtained by using a drop weight tower where a weight (30 kg) was dropped in a controlled manner on to the compression specimens. Load was monitored with the aid of a piezoelectric load transducer and charge amplifier fed into a Nicolet digital oscilloscope. Displacement immediately before and during compression was recorded using an opto-electronic transducer (namely a Fotonic sensor) and a series of accurately gridded light and dark bands attached to the drop weight. The output from this transducer was recorded simultaneously with the load data by the Nicolet.

The use of spacers between the upper and lower anvils of the drop weight compression rig enabled the specimen compression to be arrested at a desired strain value. Teflon tape was used as lubrication between the specimen ends and the anvil faces in all cases except where specifically noted.

The use of a sub-press which fully enclosed the sample enabled the specimen temperature to be varied through immersion in a water/ice bath or in a hot water bath and subsequently loaded without removing the specimen from the holder. Tests at 0° C, room temperature (20° C), 50 and 90° C were conducted.

3. Results and discussion

3.1. Appearance of a load dip during drop weight tests

Room-temperature drop weight tests on specimens having initial $h/d = 1$ produced the typical load–displacement curves shown in Fig. 1. Three characteristic

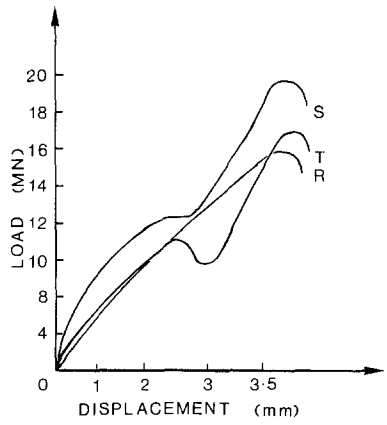

Figure 1 Typical load–displacement curves form drop weight tests. The curves are labelled R, S and T to distinguish the typical behaviour types discussed in the text. The non-linear abscissa is due to deceleration of the weight during compression.

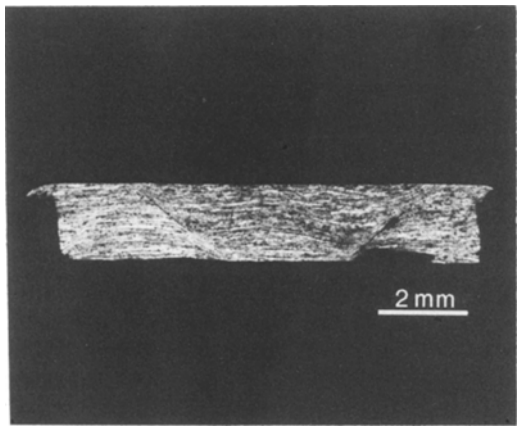

Figure 2 Cross-section of a specimen displaying a load dip. Total compressive strain = 1.03.

curves were observed. Type R showed a continuous increase in load with specimen compression, while type S displayed an intermediate stage where little or no load increase accompanied specimen compression. Type T showed a load decrease during specimen compression. Examination of specimen cross-sections parallel to the cylinder axis showed that a fracture was evident in those samples displaying a load dip, as shown in Fig. 2. It is shown below that local shear flow inhomogeneities in the form of intersecting cones, develop in all samples at a specimen height to diameter ratio of 0.5, provided that the material is work softening, i.e. the stress–strain curve exhibits negative slope. At this point the slope of the load/displacement curve is still positive, and this continues to a substantially higher strain. In most cases deformation on one of the conical inhomogeneities dominates leading eventually to the observation of curve flattening or a dip (curves S and T of Fig. 1). The dip corresponds to cases in which cracking was observed in association with the conical shear band.

The use of spacers to quickly arrest the motion of the drop weight during a test enabled specimens to be examined following compression to a desired strain value. Fig. 3a shows a drop weight test specimen deformed at room-temperature to a strain of 0.48. The broad outline of two intersecting conical shear surfaces can be distinguished from this axial section. Continued deformation usually results in one of these surfaces being favoured as shown in Fig. 3b (following a compression of $\varepsilon = 0.62$), or alternatively occasionally neither surface becomes dominant as seen in Fig. 3c (following a strain of $\varepsilon = 0.82$). In the few cases in which no conical shear surface was observed to dominate, no dip in the load displacement curve was evident (curve R of Fig. 1). If the reverse was true, a flattening or dip was observed in the load–displacement curve (types S and T of Fig. 1) and deformation appeared to localize on to one of the shear surfaces and a fracture resulted for those cases

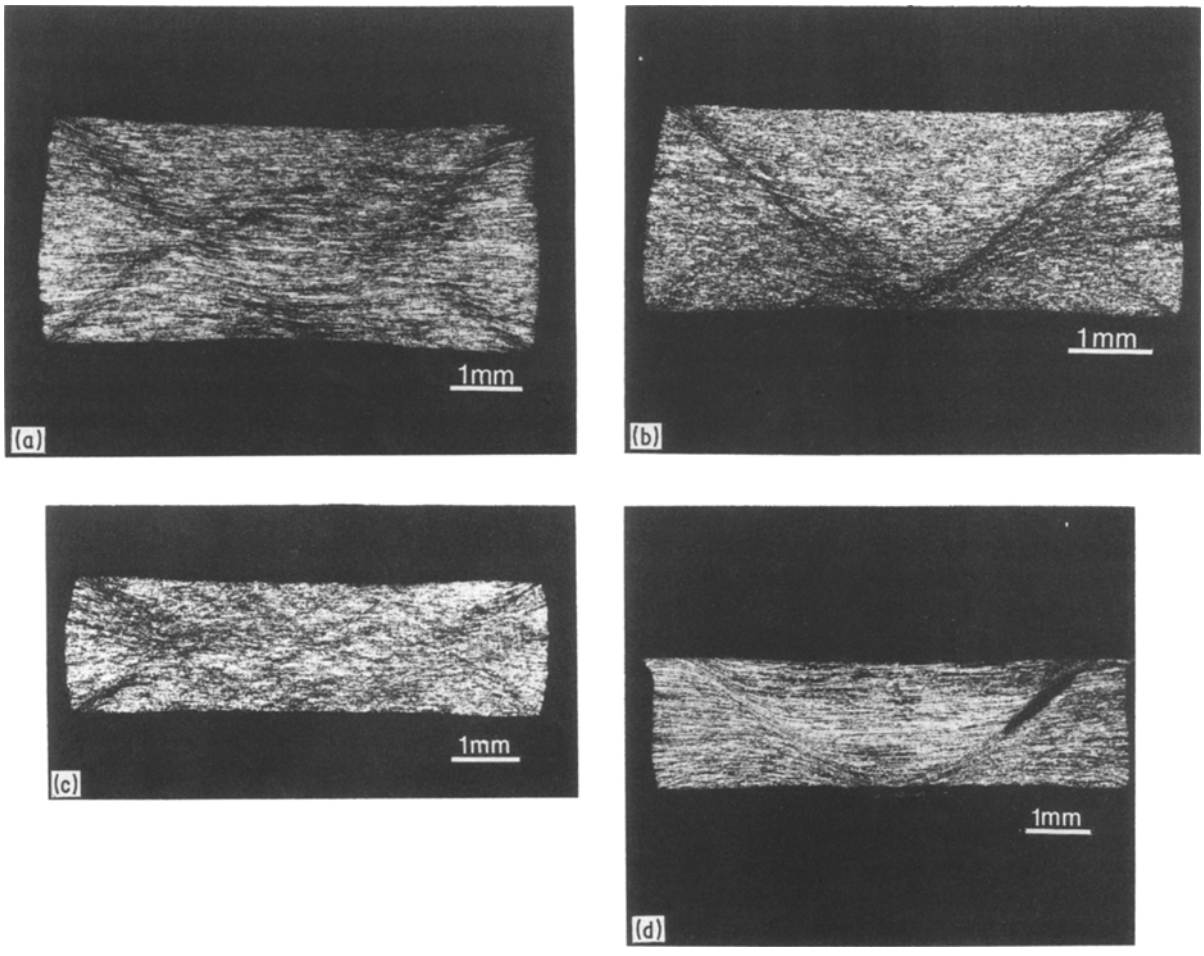

Figure 3 Cross-sections of specimens deformed in drop weight tests to strains of (a) 0.48, (b) 0.62, (c) 0.82 and (d) 0.79.

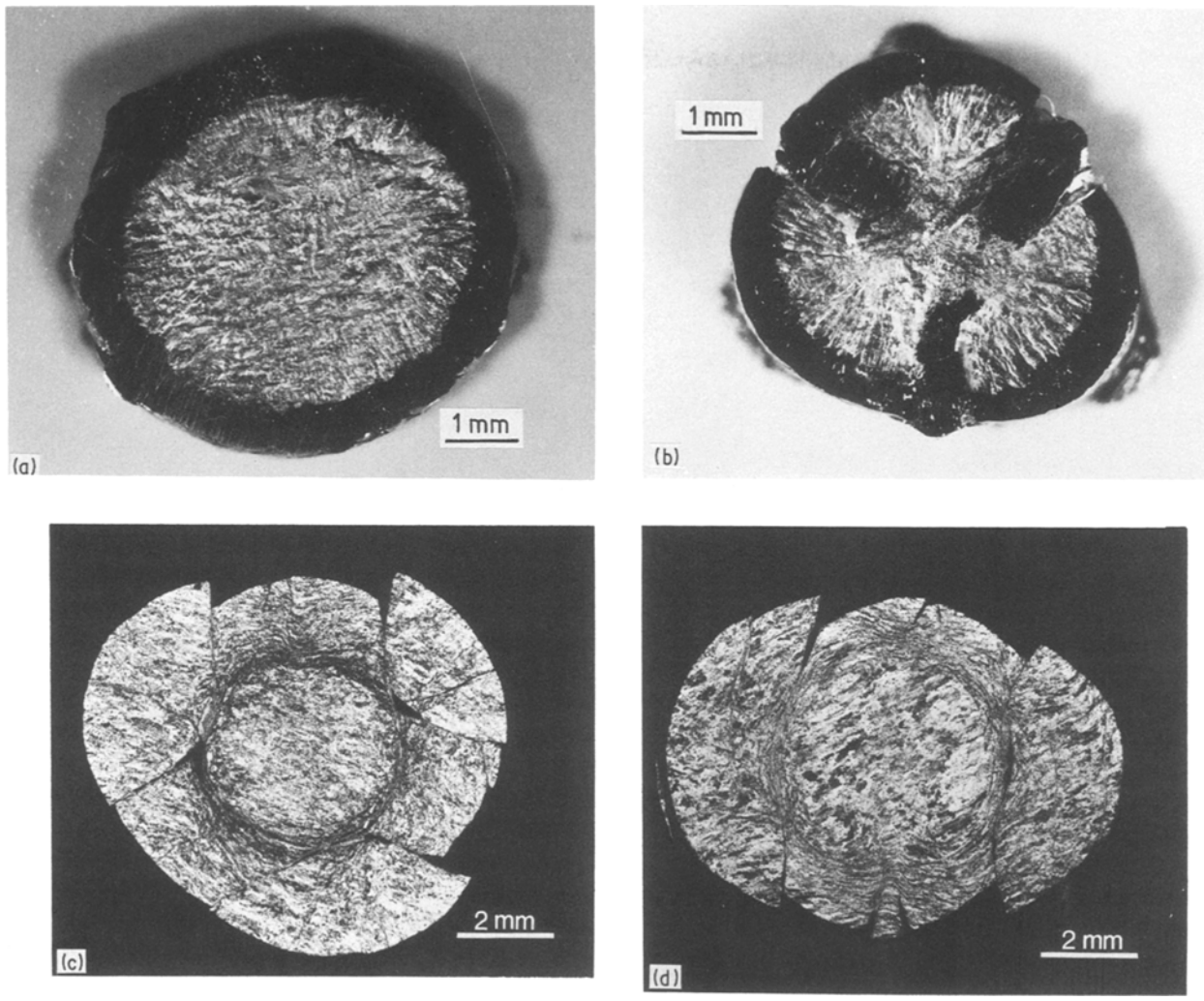

Figure 4 View of teflon-lubricated specimen surfaces following drop weight compression: (a) strain = 1.25, (b) strain = 1.03, dip observed in load–displacement curve. Both (c) and (d) show sections taken parallel to the impacted surface illustrating asymmetric shearing about a central conical shear surface.

in which a dip is observed (type T, Fig. 1) as seen in Fig. 3d, $\varepsilon = 0.79$. It is thus local concentration of deformation on to one of the conical shear surfaces and the subsequent fracture along this surface which is proposed to give rise to the dip in the load curve.

Examination of the surfaces of the test pieces where they were impacted during compression to varying strains showed, in general, a breakdown in the lubricating teflon film at the outer edges leading to direct specimen/die contact, Fig. 4a. After sufficient strain to achieve a dip in the load–displacement curve, the cracking of the sample is not axisymmetric and breakdown of the lubricant film reflects the asymmetry, Fig. 4b. Serial planar sectioning of specimens showed that the shear deformation is conical in form; however, the shear bands extend to an asymmetric cracked structure which enables the overall specimen deformation to conform to the localized deformation mode, Figs 4c and d. The nature of the asymmetric deformation is influenced by sample orientation relative to the principle directions of the original plate or bar. Fig. 5 shows a geometric reconstruction of the shear band and cracking geometry following repeated sectioning of a typical sample. The nature of the conical shear surface is evident as well as the compensating shears and cracking.

Specimens deformed in a conventional compression test at a strain rate of 1.4×10^{-4} sec^{-1} display no dip in the load–displacement curve and give rise to a stress–strain curve which remains positive, see Fig. 6. True stress–true strain curves constructed for specimens compressed in dynamic tests show a positive slope which flattens at a strain of approximately 0.30 and becomes negative for strains beyond ~ 0.39, Fig. 6. A simple calculation assuming uniform deformation, using the stress/strain properties of 2024 aluminium and thermodynamic properties from the literature [23] shows that if all the work done during compression goes into heat we would expect the stress/strain curve to become negative at $\varepsilon \sim 0.27$. The load–displacement curve, however, is expected to maintain a positive slope in compression as the sample cross-sectional area is increasing with strain. Thus the negative slope of the stress/strain curve derived from load drop test specimens is consistent with such calculations and indicates these specimens undergo thermal softening with effective negative strain hardening occurring at strains above ~ 0.39.

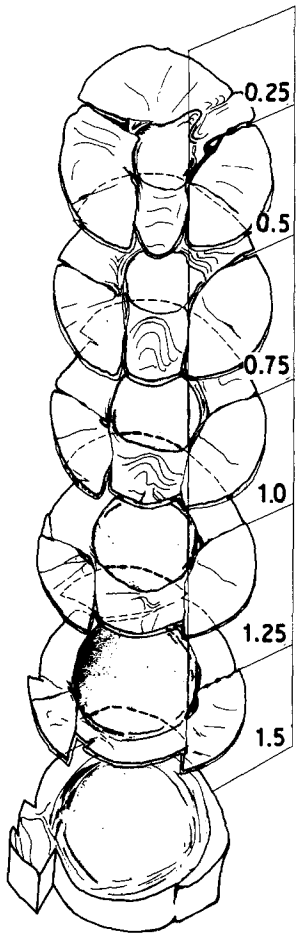

Figure 5 Reconstruction showing the appearance of shear bands, flow geometry and cracking in a series of specimen sections. The position of each section relative to the top surface of the sample is indicated in millimetres. The sample height after compression was 1.71 mm.

3.2. Development of shear surfaces and unstable flow

Fig. 3a shows a specimen having undergone uniform compression to just beyond a height to diameter ratio of $h/d = 0.5$ ($\varepsilon = 0.46$ for initial $h/d = 1$). At a strain of 0.46 the height to diameter ratio is such that according to the slipline field for compression of a slab in plane strain [22], velocity discontinuities could be expected to develop. Although this is an axisymmetric geometry, such a discontinuity is discernable here as a pair of intersecting cones. It should be noted that these shear bands are initially oriented at approximately 45°.

Further deformation in the specimen of Fig. 3a may follow one of the two paths illustrated in Fig. 7. If the shear bands are not stable, continued work hardening would cause the bands to broaden and rotate to lesser angles as the specimen is compressed and lateral spreading of the specimen occurs (Fig. 7a). On the other hand, if thermal softening is occurring when the bands initiate, the bands may become stable and allow localized deformation to continue provided material slippage at the die can occur to accommodate specimen compression. This would require the bands to remain at $\sim 45°$ whilst lateral spreading of the specimen occurred (Fig. 7b).

It is clear from Figs 3a, b and d that the latter sequence of events has dominated as the shear bands remain near to 45°. It is proposed that thermal softening is active at strain levels prior to the development of the velocity discontinuities, and that this softening stabilizes localized deformation on shear surfaces which have developed at a particular height to diameter ratio following attainment of a flow stress maximum. This is consistent with the work of Semiatin and co-workers [2, 11].

3.3. Effect of height to diameter ratio and prestrain

From geometric considerations, if the velocity discontinuity first develops at $h/d = 0.5$, we would not expect samples with initial $h/d < 0.5$ to display shear bands. Furthermore, if the presence of work softening is necessary for shear bands to stabilize, then, as work softening does not commence in these specimens until

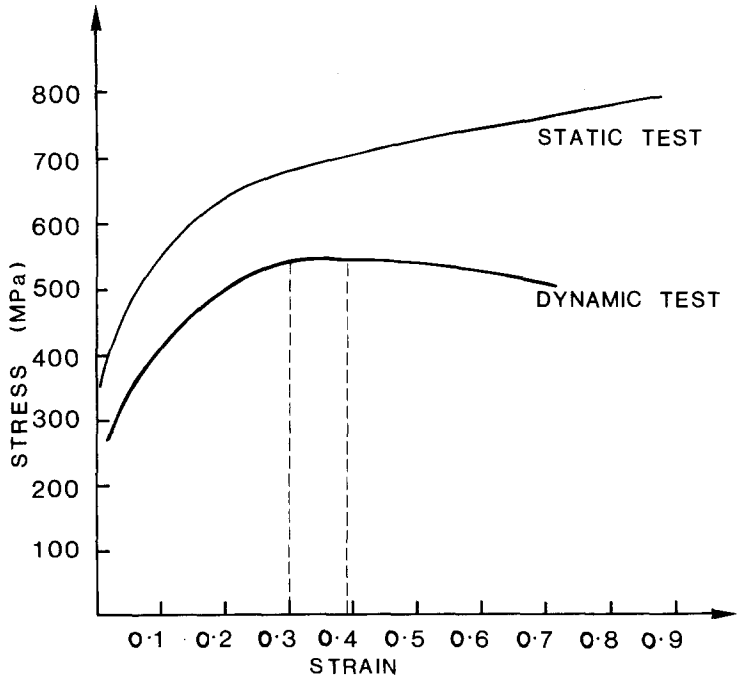

Figure 6 Typical stress/strain curves from a quasistatic compression test, $\dot{\varepsilon} \sim 10^{-4}$ sec^{-1}, and from a dynamic drop weight test, $\dot{\varepsilon} \sim 10^{2}$ sec^{-1}. Vertical lines indicate the range over which the dynamic curve levels off and becomes negative.

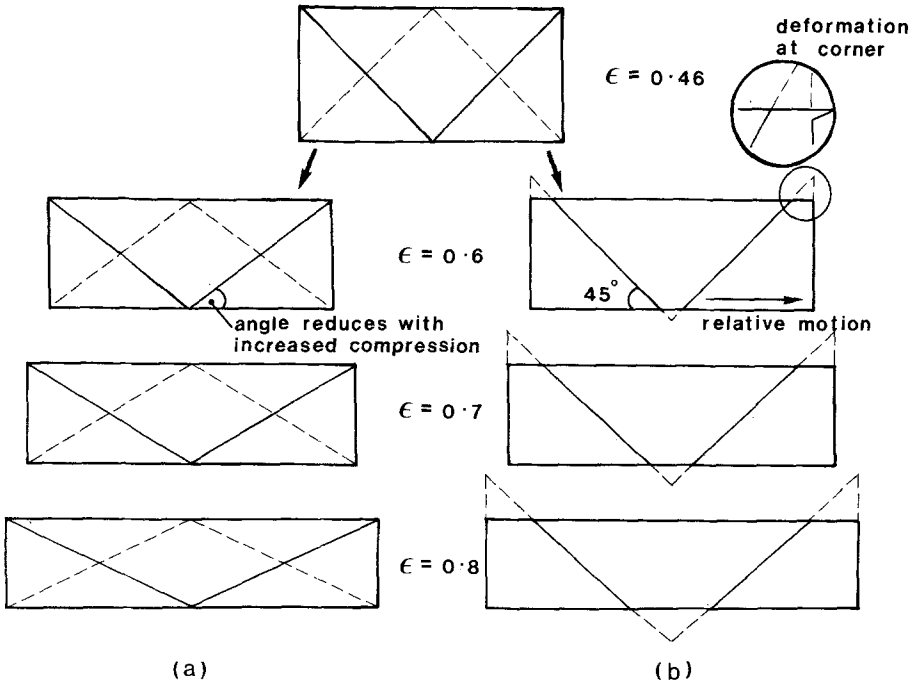

Figure 7 Schematic representation of possible shear behaviour during dynamic testing. The deformation is treated as the movement of slabs about the shear bands and the positions of the bands are indicated at four strain levels: (a) rotation of the bands and, (b) relative slipping of blocks. The required compensating deformation at the corners is indicated for (b).

$\varepsilon = 0.39 \pm 0.02$ (as shown in Fig. 6) we would not expect a load dip from samples with an initial height less than 4.1 ± 0.15 mm (initial diameter = 4.76 mm). Fig. 8 shows typical load displacement curves for a range of initial specimen heights. No load dip occurred for specimens of initial height less than or equal to 3.75 mm while specimens of initial height 4.25 mm showed evidence of load dips for some tests. Initial specimen heights greater than 4.25 mm all display a load dip associated with the development of a velocity discontinuity. These results are then consistent with the deformation bands being stabilized by thermal softening, and being initiated as velocity discontinuities at a specimen height to diameter ratio of 0.5.

In order to test the requirement that work softening is essential for the stability of shear bands once initiated, a prestrain was imposed at very slow strain rates to ensure no thermal softening would occur during this stage. For specimens of initial height 4.76 mm it is argued that because the strain at which shear band formation becomes favourable is 0.46 (i.e. $h/d = 0.5$) and thermal softening occurs following a strain of 0.39, then a pre-strain greater than 0.07 should prevent the occurrence of a load dip. Experiments showed that a prestrain of $\varepsilon = 0.20$ produced a marginal case with a dip persisting in 50% of the specimens, while a prestrain of 0.30 completely eliminated this phenomenon.

The numerical discrepancy observed here may be due to thermal softening occurring after a relatively smaller drop test strain increment due to the changed shape of the stress/strain curve following increasing levels of prestrain. Fig. 9 shows there is some variation in sample behaviour from test to test and some judgement is required to pick the strain at which softening begins. From the data it appears that work softening occurs after only $\varepsilon = 0.30$ following a prestrain of 0.20. A prestrain of 0.42 necessitated only a further strain of 0.20 at high deformation rate before softening is evident in calculated stress/strain curves. Thus these results are again consistent with the deformation banding being stabilized by thermal softening.

Contrast should be made between thermal softening being observed to stabilize velocity discontinuities as observed with the aluminium alloy in this work, and other cases exhibiting similar geometry and conditions where deformation remains substantially uniform [19]. In these latter cases the essentially uniform compressive deformation continued even though the stress/strain curves showed a negative slope. It is likely that platten/specimen friction has a dominant influence and is the reason for the observation of different forms of behaviour. For example, the deformation mode of Fig. 7b requires relative platten/specimen motion and it was found in the present tests that the base of the cone could be determined by applying the teflon lubricant to that surface only. The deformation pattern of Fig. 7b can also be achieved by rotation, at the specimen corners, of the sides into the plane of the plattens.

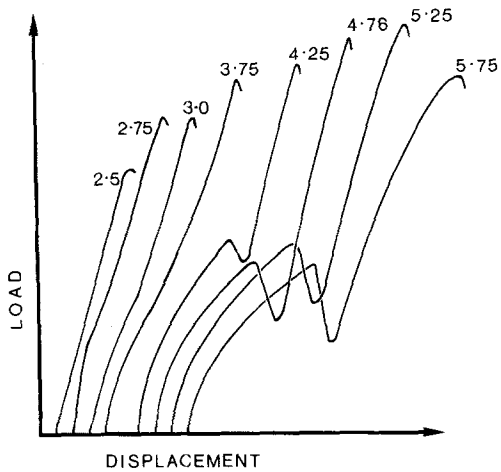

Figure 8 Typical load–displacement curves for compression specimens of initial diameter d_0 = 4.76 mm and different initial heights (indicated on the curves in millimetres).

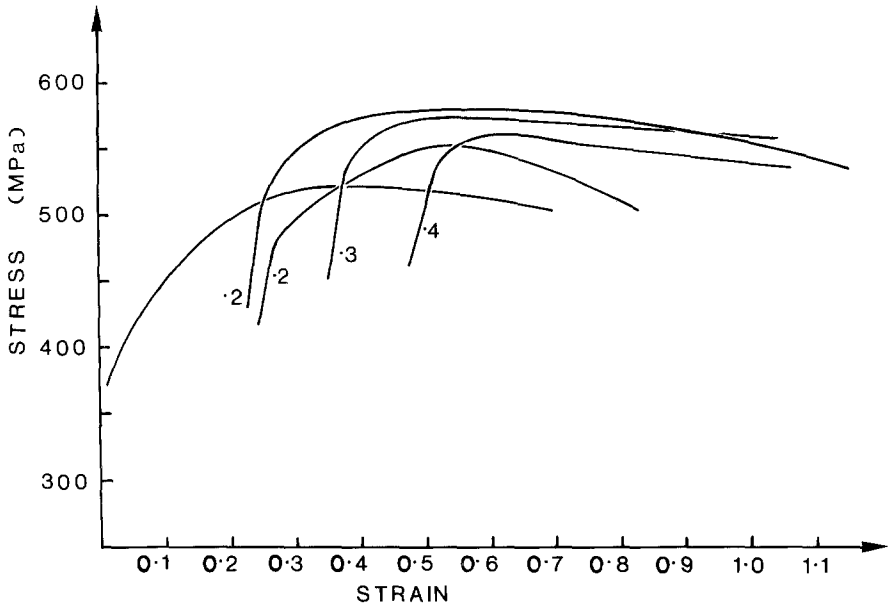

Figure 9 Dynamic stress/strain curves for specimens having undergone various levels of quasi-static pre-strain (indicated on the curves). The curves are offset by the amount of pre-strain.

3.4. Influence of temperature and sample orientation

The appearance or otherwise of a load dip could not be correlated with test temperature over the range of temperatures 0 to 90° C. In addition, no correlation was found between test temperature and the strain at which the dip occurred. It is thought that the influence of temperature on other test variables such as lubrication and the flow properties of aluminium, tends to mask its influence on the load dip mechanism. The occurrences of a load dip under various temperature and sample orientation conditions are summarized in Table I.

Tests were conducted with the axis of the cylindrical compression specimen in the short transverse (through thickness) (O), long transverse (B) and rolling (A) directions of the plate and in the axial (C), radial (E) and circumferential (D) directions of an extruded bar. The objective was to determine the influence of raw-material directional structural features, such as texture, chemical segregation and inclusion morphology, on the development of the bands and the resulting failure. The results are summarized in Table I which shows that all the sample orientations showed evidence of a dip in most of the tests conducted.

Closer examination of specimen cross-sections at higher magnifications, see Figs 10a and b, showed that inclusion strings rotate into the plane of the shear band. For orientations O, B, D and E, the orientation of the strings of inclusions relative to the direction of shear is such that they only need rotate 45° to achieve this alignment. For orientations A and C, on the other hand, a rotation of 135° is required and Figs 10a and b demonstrate that this is achieved in cases in which the samples show the instability. It is believed that fractures observed within shear bands, as seen in Figs 2 and 3d, may result from linkage of voids due to shears along strings of inclusions once aligned within the shear band. If shear remains at 45° then using the geometry of Fig. 7b, a change in the angle ($\delta\phi$) between the direction of inclusion strings crossing the band and the horizontal axis can be related to an incremental specimen height change, δh, and the band width, W, by

$$\tan(\delta\phi) = \frac{\delta h}{2^{1/2}W + \delta h} \quad (6)$$

Assuming an average band width of 0.5 mm (as measured from micrographs), rotation of inclusion strings within shear bands by 45° would necessitate an additional incremental height change of 0.81 mm. This indicates that fracture by this mechanism requires a strain of at least 0.77 for a specimen of initial height 4.76 mm (the strain to initiate the bands at a height to diameter ratio of 0.5 plus the additional strain to rotate the inclusions into the plane of the band). The occurrence of a load dip associated with the fracture is indeed observed to require approximately this amount of strain. Using this approach the strain to fracture can be calculated as a function of initial specimen height and this is shown in Fig. 11 along with the experimental data for the strain at which the instability (load dip) was observed and the theoretical curve for the strain at the onset of the velocity discontinuity at a height to diameter ratio of 0.5. In most cases the strain required is of the correct order of magnitude; however, the scatter is large and even samples with the unfavourable orientations (A and C, Table I) show the instability at a similar strain level. The reason for the scatter of results and the lack of any significant influence of specimen orientation could include variation from specimen to specimen in the band width. It is also likely that the width of the deforming region within the band reduces as straining continues, which is expected from the concept of adiabatic shear deformation.

As indicated, specimens of orientation A and C require that inclusions rotate 135° to become aligned along shear planes. Figs 10a and b shows that this is achieved in specimens which displayed fracture along the shear bands and a load dip. The strains at fracture for specimens of orientation A and C are plotted in Fig. 11 and indicated in Table I, and are not greater than the more favourably oriented samples. These

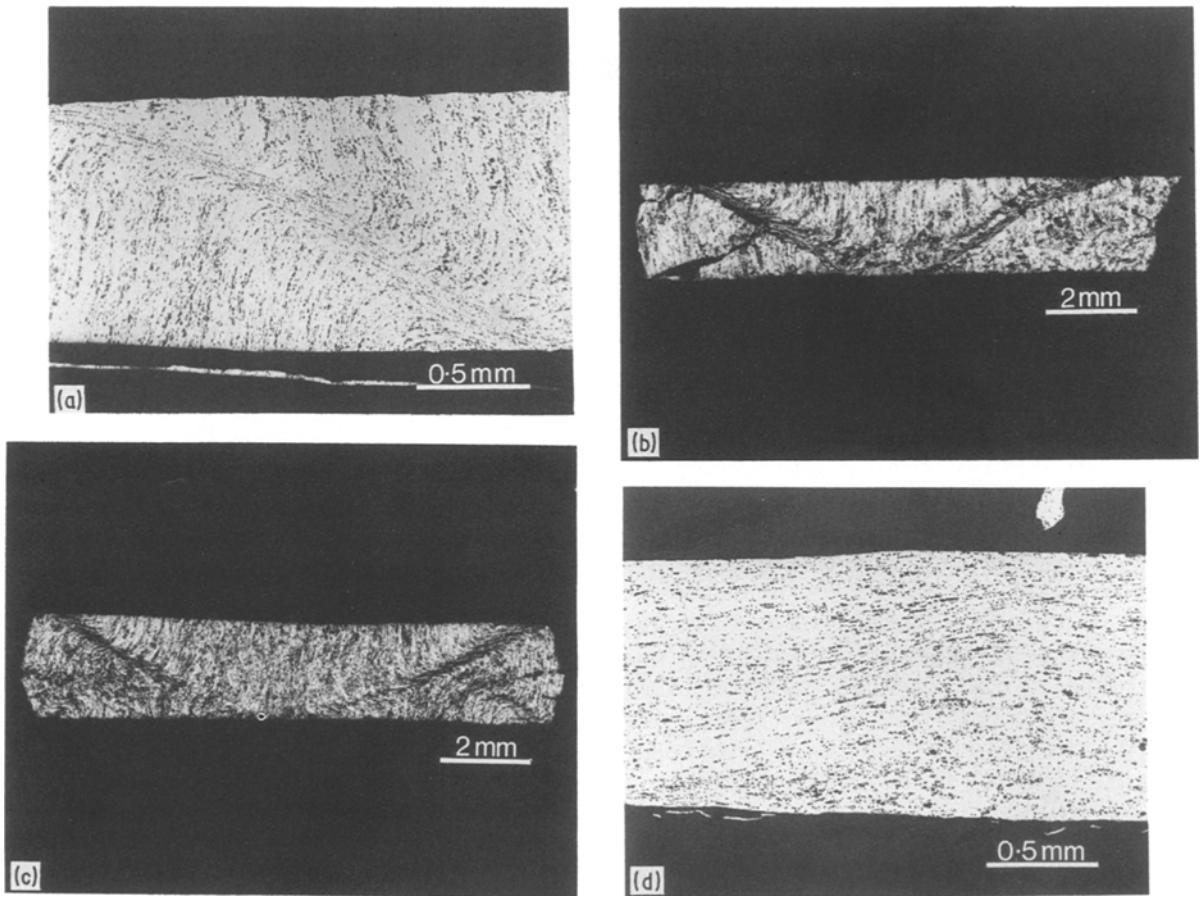

Figure 10 Micrographs of specimen cross-sections of three orientations showing the rotation of the forming directionality and inclusion alignment (the original forming directionality and inclusion alignment are parallel, thus the rotation of this directionality in (b) and (c) also indicates the rotation of the inclusions). (a) Sample orientation A, instability observed; (b) sample orientation C, instability observed; (c) sample orientation A, instability not observed; and (d) sample orientation B, instability not observed.

results suggest that inclusions are implicated in the fracture of the sample, but that the simple model using a constant band width of 0.5 mm is incorrect. Specimens of orientation A, which had not shown the instability in the load/displacement curve, when sectioned showed inclusion strings had not rotated sufficiently toward the shear band plane to lie within it, Fig. 10c; however, the rotations far exceeded 45°. In addition, specimens of the favourable orientations which do not show the instability when sectioned exhibit inclusion banding which has not rotated through 45°, Fig. 10d. The metallographic evidence implicating the inclusions with the fracture is therefore strong. An examination of the sections of Figs 2, 3, 4

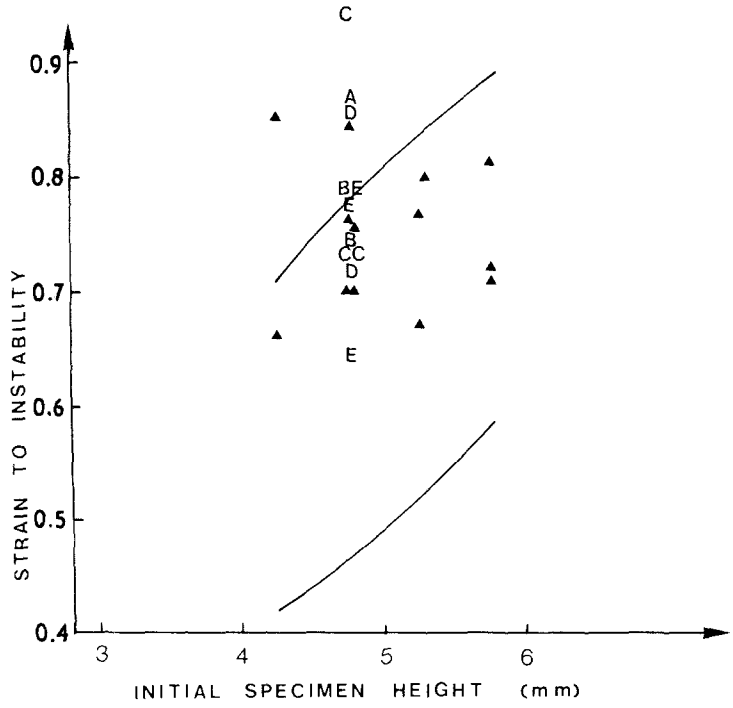

Figure 11 Plot of empirical data for the strain to fracture as a function of initial specimen height. Sample orientations are indicated by the use of a letter to plot the point except for orientation O which uses triangles, see Table I. The lower curve represents the strain at which the velocity discontinuity is expected to occur at a height to diameter ratio of 0.5, and the upper curve represents the strain at which fracture is expected for a band width of 0.5 mm and 45° rotation of inclusions to achieve fracture.

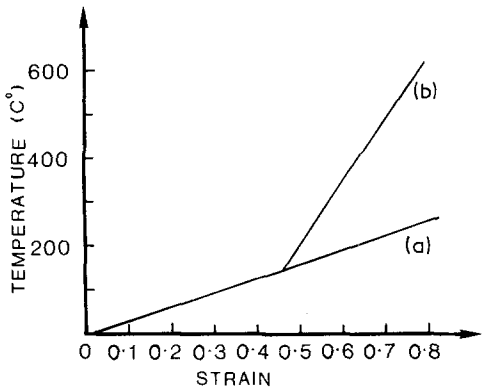

Figure 12 Calculated temperature increases expected within a sample of initial height and diameter 4.76 mm. (a) Uniform compression, (b) the temperature within the band if deformation continues within the band after it has formed at a strain of 0.46. Adiabatic conditions are assumed.

and 10 also indicates that deformation is not always clearly of the type of Fig. 7a or b, but in many cases a closer approximation to one than the other. It is considered that variations in friction conditions from test to test significantly influence the deformation mode and hence the width of and strain in the bands and the strain at which failure is observed.

Fractures were observed in sections of each sample for which a load dip occurred. It is not proven that the fracture is necessarily associated only with inclusion or segregation features rotated into the plane of the shear banding, but that if this occurs it provides one easy failure mechanism. Because of continued deformation along the bands they become thermally softened so that the reason for failure once shear bands have stabilized depends on local material properties as well as inhomogeneities. Hence the large variability observed in the strains at which failure occurs. Contributions of other mechanisms to failure must also be examined.

An assessment of the possible influence of temperature in the band deformation and failure requires an estimate of the magnitude of the temperature rise. It has been indicated that the band is stabilized by thermal softening. Using a constant flow stress of 776 MPa (ref. the quasistatic result of Fig. 6) for the aluminium and assuming adiabatic conditions, the average temperature rise in a uniformly deforming sample of initial height and diameter 4.76 mm was calculated assuming all the work of deformation is converted to heat, and is shown in Fig. 12. At strains of the order of 0.7 (near the occurrence of the dip) the temperature rises indicated are of the order of 200° C. If a band width of 0.5 mm is assumed, and uniform deformation up to a strain of 0.46 is then followed by concentrated shearing within the band, then Fig. 12 shows that at a strain of 0.7 the temperature rise in the band is of the order of 500° C; i.e. temperature in the band should approach the melting point. Whilst this is an overestimate as there will be some conduction it certainly demonstrates that severe softening will occur along the bands. Optical examination of sectioned samples shows no microcrystallization evident, and while fracture surfaces examined by scanning electron microscopy show features indicative of severe rubbing, Fig. 13, no evidence of melting was found. Thus whether or not melting has occurred locally is uncertain.

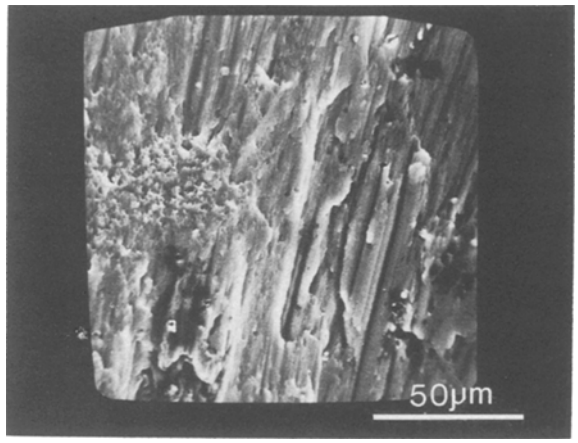

Figure 13 Typical fracture surface showing the evidence of severe rubbing typically observed.

Finally, an examination of microsections, Figs 2, 3d, 4c and d, and 10b, demonstrates very severe local distortions. Thus a contribution to fracture will involve exhaustion of aluminium matrix ductility as well as the influences of inclusions and temperature rise discussed above.

4. Conclusions

1. Drop weight compression tests on right circular cylindrical specimens of 2024 aluminium revealed a failure occurring through strain localization on shear bands of conical geometry.

2. A dip in the load–extension curve is associated with a fracture occurring in the plane of the shear band.

3. The effect of testing temperature on shear band development was not clear, possibly being obscured by the temperature dependence of both the mechanical properties of the 2024 aluminium and of the lubrication used (PTFE film).

4. Tests on specimens with different initial height to diameter ratios indicate that the development of shear bands is initiated by a velocity discontinuity at a specimen height to diameter ratio of 0.5. These tests also demonstrated that thermal softening is essential to stabilize deformation on the shear surface and that sufficient strain is required to achieve thermal softening before the sample reaches the critical height to diameter ratio.

5. Tests on specimens having undergone varying levels of pre-strain at slow strain rate support the necessity for thermal softening to occur in order to stabilize flow on shear surfaces.

6. Tests on specimens of different orientations show the tendency for inclusion strings to rotate into the plane of the shear surface. For all fractures observed in cross-section, these inclusion strings were noted to lie near the shear direction where they crossed the shear bands. Specimens not exhibiting fracture show these inclusions to have rotated but not so far as to lie in the shear direction.

7. The cause of the fracture along shear planes could not be isolated to the inclusion strings and both

thermal softening and exhaustion of matrix aluminium ductility are expected to contribute to the fractures.

Acknowledgement

Mr P. McCarthy's assistance in preparing and photographing the metallographic sections is greatly appreciated.

References

1. S. L. SEMIATIN and J. J. JONAS, "Formability and Workability of Metals" (ASM, Metals Park, Ohio, 1984).
2. S. L. SEMIATIN, G. D. LAHOTI and S. I. OH, in Proceedings 29th Sagamore Army Materials Research Conference (Plenum, New York, 1983) p. 119.
3. A. J. BEDFORD, A. L. WINGROVE and K. R. L. THOMPSON, *J. Aust. Inst. Met.* **19** (1974) 61.
4. H. C. ROGERS, "Adiabatic Shearing, a Review" (Drexel University, Philadelphia, Pennsylvania, for US Army Research Office, May 1974).
5. H. C. ROGERS, *Ann. Rev. Mater. Sci.* **9** (1979) 283.
6. G. B. OLSEN, J. F. MESCALL and M. AZRIN, in "Shock Waves and High-Strain-Rate Phenomena in Metals", edited M. A. Meyers and L. L. Murr (Plenum, New York, 1980) p. 221.
7. H. C. ROGERS, in Proceedings 29th Sagamore Army Materials Research Conference (Plenum, New York, 1983) p. 101.
8. C. ZENER and J. H. HOLLOMON, *J. Appl. Phys.* **15** (1944) 22.
9. R. F. RECHT, *J. Appl. Mech. Trans. ASME* **31E** (1964) 189.
10. M. R. STAKER, *Acta Metall.* **29** (1981) 683.
11. S. L. SEMIATIN and G. D. LAHOTI, *Met. Trans. A* **12A** (1981) 1719.
12. *Idem, ibid.* **14A** (1983) 105.
13. *Idem, ibid.* **13A** (1982) 275.
14. J. F. MESCALL, R. PAPIRNO and J. McLAUGHLIN, in "Compression Testing of Homogeneous Materials and Composites", edited by R. Chait and R. Papirno, ASTM STP 808 (American Society for Testing and Materials, Philadelphia, Pennsylvania, 1983) p. 7.
15. Z. DARVAS, *Mater. Sci. Engng* **70** (1985) 101.
16. R. PAPIRNO, J. F. MESCALL and A. M. HANSEN, in "Compression Testing of Homogeneous Materials and Composites", edited by R. Chait and R. Papirno, ASTM STP 808 (American Society for Testing and Materials, Philadelphia, Pennsylvania, 1983) p. 40.
17. G. L. WULF, *Int. J. Mech Sci.* **20** (1978) 609.
18. J. L. AFFOUARD, R. DORMEVAL, M. STELLY and J. P. ANSART, in Proceedings 3rd Conference on Mechanical Properties of Materials at High Rates of Strain, Oxford, (Institute of Physics, Conference Series No. 70) (1984) p. 533.
19. R. L. WOODWARD, N. J. BALDWIN, I. BURCH and B. J. BAXTER, *Met. Trans. A* **16A** (1985) 2031.
20. S. KOBAYASHI, C. H. LEE, Y. SAIDA and S. C. JAIN, "Analytical Prediction of Defects Occurrence in Simple and Complex Forgings", Technical Report AFML-TR-70-90 (July 1970).
21. S. KOBAYASHI, S. SOHRABPOUR and M. M. SEHGAL, "Study of Deformation and Defects Occurrence in Advanced Forging Technique", Technical Report AFML-TR-71-69 (September 1971).
22. A. B. WATTS and H. FORD, *Proc. Inst. Mech. Eng.* **1B** (1952–3) 448.
23. "Metals Handbook", 9th Edn, Vol. 2, "Properties and Selection of Non Ferrous Alloys and Pure Metals" (ASM, Metals Park, Ohio, 1979) p. 57.

Received 7 September
and accepted 10 December 1987